Nature of Prominences and their role in Space Weather
Proceedings IAU Symposium No. 300, 2013
B. Schmieder, J.-M. Malherbe & S. T. Wu, eds.

doi:10.1017/S1743921313010843

Modeling Magnetic Flux Ropes

Chun Xia and Rony Keppens

Centre for mathematical Plasma Astrophysics, KU Leuven,
email: chun.xia@wis.kuleuven.be

Abstract. The magnetic configuration hosting prominences can be a large-scale helical magnetic flux rope. As a necessary step towards future prominence formation studies, we report on a stepwise approach to study flux rope formation. We start with summarizing our recent three-dimensional (3D) isothermal magnetohydrodynamic (MHD) simulation where a flux rope is formed, including gas pressure and gravity. This starts from a static corona with a linear force-free bipolar magnetic field, altered by lower boundary vortex flows around the main polarities and converging flows towards the polarity inversion. The latter flows induce magnetic reconnection and this forms successive new helical loops so that a complete flux rope grows and ascends. After stopping the driving flows, the system relaxes to a stable helical magnetic flux rope configuration embedded in an overlying arcade. Starting from this relaxed isothermal end-state, we next perform a thermodynamic MHD simulation with a chromospheric layer inserted at the bottom. As a result of a properly parametrized coronal heating, and due to radiative cooling and anisotropic thermal conduction, the system further relaxes to an equilibrium where the flux rope and the arcade develop a fully realistic thermal structure. This paves the way to future simulations for 3D prominence formation.

Keywords. Sun: prominences, filaments — MHD

Helical magnetic flux ropes are the most promising magnetic structures for solar prominences and their surrounding coronal cavities. More and more evidence for their existence is found in various observations (Gibson *et al.* 2010), with especially the latest observations using coronal magnetometry on cavities (Bak-Stęślicka *et al.* 2013) showing twist or shear of magnetic field extending up into the cavity and a pattern of concentric rings in line-of-sight velocity. Analytical models (Low & Zhang 2004) and numerical models (Fan 2010) of magnetic flux ropes have been proposed to explain observations on prominences and cavities. The physical processes that generate magnetic flux ropes in the corona are studied by many models based on magnetic flux cancellation in the photosphere. Many of these models focus on the magnetic structure alone and realistic temperature and density structures are missing.

To understand the formation process of a flux rope and to ultimately build a realistic model to explain prominences and cavities, we decouple the huge challenge of prominence formation modeling into two stages: (1) creating a magnetic flux rope from physically meaningful processes including gas pressure and gravity effects; (2) simulating the prominence plasma formation inside the pre-existing flux rope by including thermodynamics and chromospheric evaporation. This two-step approach is justified since the time scales for radiative processes that trigger condensations forming prominence plasma are much shorter than those of the large-scale evolution of the magnetic field.

1. First stage

We here summarize our recent results, discussed more extensively in Xia *et al.* 2013. In a 3D Cartesian box with extension of $-120 < x < 120$ Mm, $-90 < y < 90$ Mm, and $3 < z < 123$ Mm, an initial magnetic field adopts a linear force-free field extrapolation

from an analytic bipolar magnetogram $B_z^0(x,y)$. In this first stage, we use an isothermal assumption with temperature $T_0 = 1$ MK throughout the domain representing the solar corona and solve the following isothermal MHD equations:

$$\frac{\partial \rho}{\partial t} + \nabla \cdot (\rho \mathbf{v}) = 0, \tag{1.1}$$

$$\frac{\partial (\rho \mathbf{v})}{\partial t} + \nabla \cdot \left(\rho \mathbf{v}\mathbf{v} + p_{\rm tot}\mathbf{I} - \frac{\mathbf{B}\mathbf{B}}{\mu_0} \right) = \rho \mathbf{g} - \nabla \cdot \Pi, \tag{1.2}$$

$$\frac{\partial \mathbf{B}}{\partial t} + \nabla \cdot (\mathbf{v}\mathbf{B} - \mathbf{B}\mathbf{v}) = 0, \tag{1.3}$$

where ρ, $\mathbf{v}$, $\mathbf{B}$, and $\mathbf{I}$ are the plasma density, velocity, magnetic field, and unit tensor, respectively, while the total pressure is $p_{\rm tot} \equiv p + \frac{B^2}{2\mu_0}$ and $\mathbf{g} = -g_\odot r_\odot^2/(r_\odot + z)^2 \hat{\mathbf{z}}$ is the solar gravitational acceleration. A stress tensor Π incorporates viscous effects. The code we use is the parallelized Adaptive Mesh Refinement Versatile Advection Code (MPI-AMRVAC, Keppens *et al.* 2012). A third-order accurate, shock-capturing scheme is used. The usage of a three-level AMR grid gives an effective resolution of $512 \times 384 \times 256$ and has a spatial resolving ability of 469 km. The initial density is derived from hydrostatic equilibrium under gravity.

To adjust the initial magnetic arcade to become more realistic, we impose a twisting velocity field, which is composed of two large-scale vortices rotating around the two main polarities, in the bottom plane. The normal velocity at the bottom is kept zero, and also on the other faces of the box, we keep zero velocity during this phase. The magnetic field on the boundaries is extrapolated by one-sided finite differencing. We use zeroth order extrapolation for the density on side boundaries, fixed density at the bottom, and adopt a gravitationally stratified density profile at the top. After the bottom driving and a relaxation, the lower smaller loops are further sheared while the overlying larger loops become less sheared and closer to potential field (see Fig. 1(a)(b)).

After this adjustment, we impose a converging velocity field toward the polarity inversion line (PIL) on the bottom boundary with the horizontal velocity formulated as

$$v_x^b = -f(t) v_1 \frac{\partial |B_z^0(x,y)|}{\partial x} \exp(-y^2/y_d^2),\ v_y^b = -f(t) v_1 \frac{\partial |B_z^0(x,y)|}{\partial y} \exp(-y^2/y_d^2), \tag{1.4}$$

where $y_d = 50$ Mm, $f(t)$ is a linear function to switch the driving on and off smoothly and the amplitude v_1 keeps the driving speed below 2% of the initial local Alfvén speed. We keep zero velocity on the four side boundaries and adopt limited open boundary conditions at the bottom and the top boundaries by extrapolations ensuring zero normal-gradient velocity and by setting an upper limit of 10% of the local Alfvén speed on the normal velocity. Similarly, the speed of downflows through the bottom is limited to be smaller than 1% of the local Alfvén speed. The density on the bottom boundary is extrapolated by gravitational stratification and kept no less than its initial value. Other boundary conditions are the same as the previous phase. The converging flows drive the system for 50 minutes before they cease. The system relaxes to a stable state over 60 minutes with zero horizontal velocity at the bottom.

The converging flows drive the footpoints of magnetic loops to approach the polarity inversion line (PIL), and the loops get sheared even further. In locations near the PIL, magnetic loops are brought closer to be parallel to the PIL. Flux elements of opposite polarities, where the loops are rooted in, are forced to collide at the PIL, and magnetic reconnection occurs there. As a result, pairs of arched magnetic loops, originally separate in x-extension, now become linked together in a head-tail style. The end result produces long helical flux tubes which have a concave magnetic dip at their middle portion and

https://doi.org/10.1017/S1743921313010843 Published online by Cambridge University Press

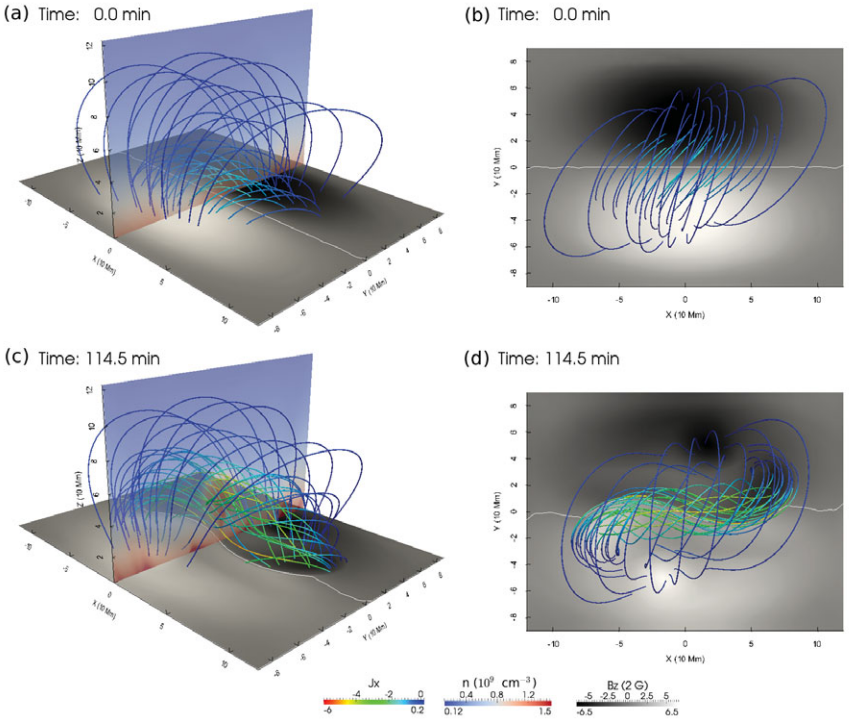

Figure 1. Adjusted sheared magnetic arcade (upper panels) and the stable magnetic flux rope (lower panels). The bottom magnetograms are shown in gray with the PIL plotted in white. Magnetic field lines are colored by x-component of the local current density J_x in the rainbow color table. The vertical planes are colored by number density in blue-red colors. Side views and top views are shown in the left and right column respectively. Adopted from Xia *et al.* 2013.

hence ascend due to magnetic tension. The shorter reconnected loops which form below the reconnection sites, sink down through the bottom, causing magnetic flux cancellation. As the driving continues, new helical flux tubes form and wrap around prior-formed ones and together they assemble into a large scale helical flux rope. This is then found to rise, expand, stretch overlying loops, and relax to a stable state (see Fig. 1(c)(d)).

2. Second stage

To use an evaporation-condensation model to produce prominences (as in previous 2.5D work in Xia *et al.* 2012), a chromospheric layer must be included with temperature and density stratification, and thermodynamics must be considered. In this stage, we extend the isothermal MHD to thermodynamic MHD by adding the following energy equation:

$$\frac{\partial E}{\partial t} + \nabla \cdot \left(E\mathbf{v} + p_{\rm tot}\mathbf{v} - \frac{\mathbf{BB}}{\mu_0} \cdot \mathbf{v} \right) = \rho \mathbf{g} \cdot \mathbf{v} + \nabla \cdot (\boldsymbol{\kappa} \cdot \nabla T) - Q + H, \qquad (2.1)$$

where $p_{\rm tot} \equiv p + B^2/(2\mu_0)$ is the total pressure, composed of gas pressure p and magnetic pressure $B^2/(2\mu_0)$; $E = p/(\gamma - 1) + \rho v^2/2 + B^2/(2\mu_0)$ is the total energy density and adiabatic index $\gamma = 5/3$. The last three terms stand for thermal conduction, radiative cooling, and coronal heating respectively.

https://doi.org/10.1017/S1743921313010843 Published online by Cambridge University Press

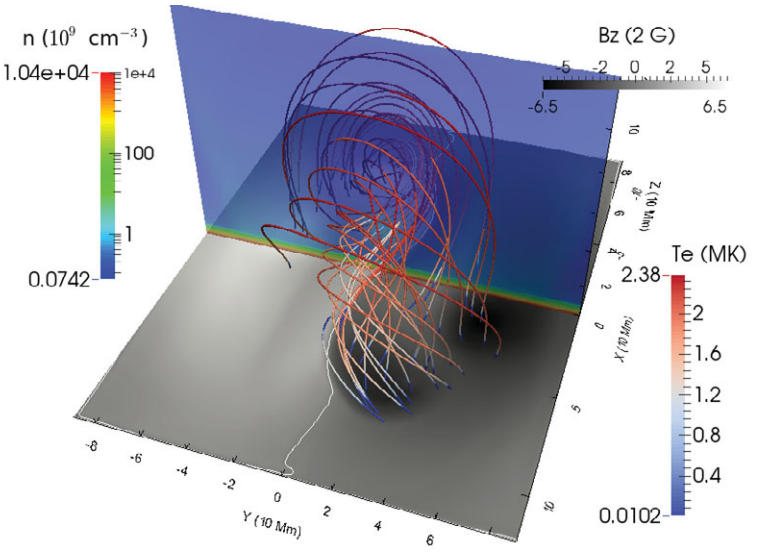

Figure 2. The stable flux rope in stratified solar atmosphere with magnetic field lines colored by temperature T_e and a translucent vertical cut colored by number density n.

To start a full MHD simulation from the isothermal MHD data at the end of the first stage with a stable flux rope in the corona, we calculate gas pressure from the density distribution and constant 1 MK temperature and hence obtain the total energy E. In the bottom layer from 3 Mm to 7 Mm, the constant temperature is replaced by a hyperbolic tangent profile, where a region at 10000 K in the chromosphere (with thickness of 3 Mm) connects to the 1 MK in the corona. The number density in this layer is then determined by assuming a hydrostatic atmosphere with the bottom value of 10^{13} cm^{-3}. We restart the simulation from this modified end state of the first stage using MPI-AMRVAC, and relax the system towards an equilibrium with a time-dependent coronal heating. The latter contains a cosine function of time during the first 57 minutes, tuning the heating from 2×10^{-4} to 6×10^{-5} erg cm^{-3} s^{-1} and maintained constant since then. After a relaxation of about 100 min, this full thermodynamic MHD system reaches a quasi-equilibrium with residual velocity smaller than 10 km s^{-1}. Representative field lines colored by temperature and a central vertical slice colored by density are shown in Fig. 2. The dipped parts of the helical loops in the lower part of the flux rope are cooler, at around 0.8 MK. The top of the flux rope and the large arcade loops are hotter, about 2.4 MK.

Summarizing, we presented successive stages of simulations with isothermal MHD followed by thermodynamic MHD approaches, to finally get a realistic filament channel with a magnetic flux rope from chromosphere up to corona. From this state, a prominence formation inside the flux rope can be simulated in the future.

References

Bak-Stęślicka, U. *et al.* 2013, *ApJ*, 770, L28
Fan, Y. 2010, *ApJ*, 719, 728
Gibson, S. E. *et al.* 2010, *ApJ*, 724, 1133
Keppens, R. *et al.* 2012, *J. Comput. Phys.*, 231, 718
Low, B. C. & Zhang, M. 2004, *ApJ*, 609, 1098
Xia, C., Chen, P. F., & Keppens, R. 2012, *ApJ*, 748, L26
Xia, C., Keppens, R., & Guo Y. 2013, *ApJ*, submitted

https://doi.org/10.1017/S1743921313010843 Published online by Cambridge University Press